Parity nonconservation in ^{106}Pd and ^{108}Pd neutron resonances

B. E. Crawford,[1,*] J. D. Bowman,[2] P. P. J. Delheij,[3] T. Haseyama,[4] J. N. Knudson,[2] L. Y. Lowie,[5,†] A. Masaike,[4,‡] Y. Matsuda,[4,§] G. E. Mitchell,[5] S. I. Penttilä,[2] H. Postma,[6] N. R. Roberson,[1] S. J. Seestrom,[2] E. I. Sharapov,[7] S. L. Stephenson,[5,*] and V. W. Yuan[2]

[1]*Duke University, Durham, North Carolina 27708*
and Triangle Universities Nuclear Laboratory, Durham, North Carolina 27708-0308
[2]*Los Alamos National Laboratory, Los Alamos, New Mexico 87545*
[3]*TRIUMF, Vancouver, British Columbia, Canada V6T 2A3*
[4]*Physics Department, Kyoto University, Kyoto 606-01, Japan*
[5]*North Carolina State University, Raleigh, North Carolina 27695-8202*
and Triangle Universities Nuclear Laboratory, Durham, North Carolina 27708-0308
[6]*Delft University of Technology, Delft, 2629 JB, The Netherlands*
[7]*Joint Institute for Nuclear Research, 141980 Dubna, Russia*

(Received 8 July 1999; published 19 October 1999)

Parity nonconservation (PNC) has been studied in the neutron *p*-wave resonances of ^{106}Pd and ^{108}Pd in the energy range of 20 to 2000 eV. Longitudinal asymmetries in *p*-wave capture cross sections are measured using longitudinally polarized neutrons incident on ~20-g metal-powder targets at LANSCE. A CsI γ-ray detector array measures capture cross section asymmetries as a function of neutron energy which is determined by the neutron time-of-flight method. A total of 21 *p*-wave resonances in ^{106}Pd and 21 *p*-wave resonances in ^{108}Pd were studied. One statistically significant PNC effect was observed in ^{106}Pd, and no effects were observed in ^{108}Pd. For ^{106}Pd a weak spreading width of $\Gamma_w = 34^{+47}_{-28} \times 10^{-7}$ eV was obtained. For ^{108}Pd an upper limit on the weak spreading width of $\Gamma_w < 12 \times 10^{-7}$ eV was determined at the 68% confidence level.
[S0556-2813(99)05311-X]

PACS number(s): 24.80.+y, 25.40.Ny, 27.60.+j, 11.30.Er

I. INTRODUCTION

Since the discovery of large parity nonconserving (PNC) effects in compound nuclear resonances by Alfimenkov *et al.* [1] at Dubna, interest has focused on the compound nucleus as a laboratory for studying not only the weak interaction itself but also the role of parity nonconservation in our understanding of nuclear structure [2]. The Dubna group measured the longitudinal asymmetries in *p*-wave resonances by neutron transmission through a variety of targets, observing asymmetries as large as 7% with neutron energies up to 10 eV.

Parity nonconservation arises from the mixing of *s*- and *p*-wave neutron resonances and results in a helicity dependence in the total *p*-wave cross section for longitudinally polarized neutrons incident on unpolarized targets. The helicity dependent cross section is given by

$$\sigma_p^{\pm} = \sigma_p(1 \pm f_n P), \tag{1}$$

where σ_p is the unpolarized cross section and f_n is the degree of neutron polarization. By measuring the helicity dependent asymmetry in the *p*-wave cross section, one determines the PNC asymmetry *P*.

The main limitation of the work by the Dubna group is the narrow energy range, restricting the measurement to only a few resonances per nucleus. Because of the statistical nature of the compound nucleus it is desirable to measure several PNC asymmetries in each nucleus studied. Using the high-flux, pulsed, epithermal neutron facility at the Los Alamos Neutron Science Center (LANSCE) and the apparatus described below, the TRIPLE (time reversal and parity at low energies) Collaboration developed a system to extend the energy range of these measurements to significantly increase the number of resonances studied in each nucleus. In addition, the TRIPLE Collaboration developed analysis techniques which exploit the statistical nature of the compound nucleus [3,4]. From the collection of measured PNC-asymmetry values our analysis extracts the root-mean-squared parity-nonconserving matrix element *M* for the given nuclide. In order to compare PNC matrix elements from different nuclei, one forms a weak spreading width

$$\Gamma_w = \frac{2\pi M^2}{D}, \tag{2}$$

where *D* is the energy spacing between levels with the same spin for the nuclide in question. By analogy with similar studies with isospin [5] it is expected that Γ_w is essentially constant as a function of nuclear mass, although local fluctuations are possible [6,7]. The TRIPLE Collaboration has focused its efforts in two regions of the periodic chart, places

*Present address: Gettysburg College, Gettysburg, PA 17325.
†Present address: McKinsey and Company, Atlanta, GA 30303.
‡Present address: Fukui University of Technology, 3-6-1 Gakuen, Fukui-shi 910-8505, Japan.
§Present address: Institute of Physical and Chemical Research (RIKEN), Saitama 351-0198, Japan.

 ©1999 The American Physical Society

where the *p*-wave strength function peaks, the mass-100 and mass-230 regions. The current measurements are part of an effort to determine Γ_w in the mass-100 region. Results of studies with several targets have recently been published: ^{238}U [8], ^{232}Th [9], ^{113}Cd [10], ^{107}Ag, and ^{109}Ag [11], ^{93}Nb [6], ^{133}Cs [7], and ^{103}Rh [12].

The traditional transmission experiments use large (several kg) targets, and the difference in neutron transmission between positive and negative helicity neutrons is measured. However, it is not always possible to obtain isotopically pure targets of sufficient mass to perform a transmission experiment. For small areal density isotopically pure targets, the capture method has been shown to be more sensitive than transmission measurements for observing both the *p*-wave resonances themselves and the parity nonconserving asymmetries in these resonances [13,14].

II. EXPERIMENTAL APPARATUS

The experiments are performed on flight path 2 at the Manuel Lujan Jr. Neutron Scattering Center (MLNSC). An overview of much of the apparatus is given in Ref. [15].

An 800-MeV proton beam from the LANSCE linac is bunched and stored in a proton storage ring (PSR) forming a 20-Hz pulsed beam with an average current of 70 μA. The shape of the beam pulse is that of an isosceles triangle with a base of 250 ns. After exiting the PSR, the protons are deposited on a pair of tungsten spallation targets producing approximately 17 neutrons for each incident proton. A water moderator is used to produce thermal and epithermal energy neutrons [16]. Each neutron pulse, therefore, contains a range of energies. The TRIPLE beam line shown in Fig. 1 uses a 60-m flight path to separate the neutron energies by the neutron time-of-flight method.

The pulsed epithermal neutron beam is monitored by a pair of ^{3}He and ^{4}He ionization chambers. Since both chambers are sensitive to γ-rays, but only the ^{3}He chamber is sensitive to neutrons, a subtraction of the two signals measures the incident flux. The monitors do not provide an absolute measurement of the flux but rather monitor the stability of the incoming beam.

The neutrons pass through a dynamically polarized proton target that is cooled to 1 K in a 5-T magnetic field [17]. The resulting neutron beam is polarized to $\sim$85% by the spin-dependent scattering of the unpolarized neutrons by the polarized protons.

The neutron spin direction is reversed every 10 s by a spin flipper composed of a system of longitudinal and transverse magnetic fields [18]. Turning off or on a transverse magnetic field, the spin flipper either leaves the neutrons polarized along the beam direction or adiabatically rotates the spins to the opposite direction. The efficiency of adiabatic rotation of the neutrons is discussed in Ref. [18] and is essentially constant from 1 eV to several hundred eV.

Since the Earth's magnetic field will precess the neutron spins during the 60-m flight path and thus depolarize the beam, a 10-G solenoidal field is used to preserve the longitudinal spin of the neutrons. The depolarization due to the combination of the Earth's magnetic field and the discontinuities in the solenoidal windings is discussed in Ref. [19] and is on the order of a few percent.

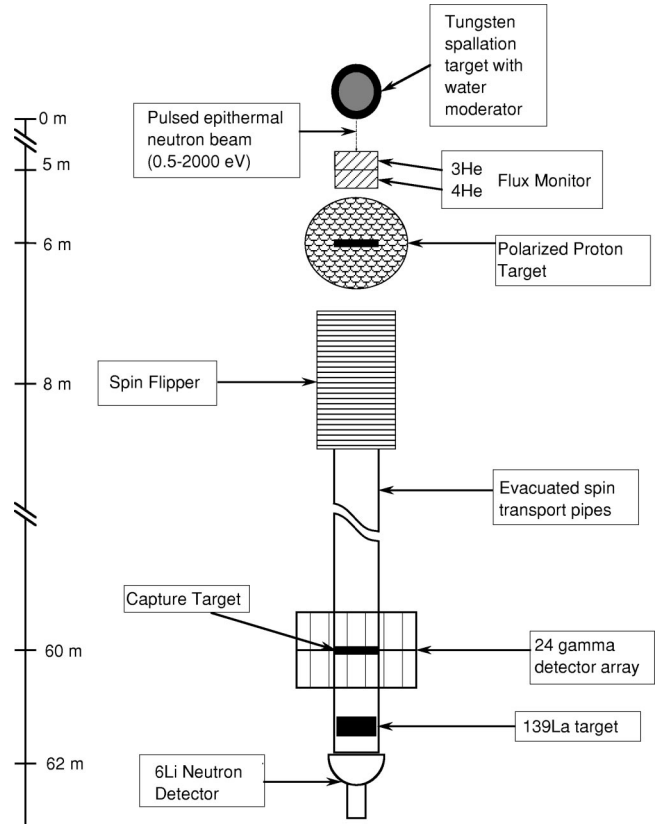

FIG. 1. Schematic of the TRIPLE beam line set up for a capture γ-ray measurement.

The neutron energy is determined by the time-of-flight method, where the neutrons are ''detected'' by measuring the γ rays produced during neutron capture in the target. The capture γ-ray detector consists of 24 15-cm long CsI crystal wedges that form two annular rings of 12 sections each. The target sits at the center of the two rings such that the total solid angle of the detector is 85% of 4π. A 5-cm thick cylinder of ^{6}Li-loaded polyethylene between the target and detector shields the neutron-sensitive CsI crystals from scattered neutrons. Signals from the up-stream and down-stream halves of the detector are combined so that electronically the detector consists of one 12-detector ring. The detector signals are shaped by 30-ns passive filters to aid in signal discrimination by constant fraction discriminators (CFDs) which are set with a threshold corresponding to a γ-ray energy of 0.3 MeV. The CFD outputs are cabled to the data room where the signals are rediscriminated and fed into a linear summer. The linear sum of the 125-ns wide pulses are then discriminated at a voltage level such that only events with two or more pulses in coincidence are counted. Thus we reduce our background signal by requiring a γ multiplicity of 2. The output of this last discriminator is shaped by a 100-ns filter and fed to a transient digitizer which samples the combined detector signal every 100 ns. This results in an 8192-channel γ-ray spectrum. A typical γ-ray spectrum after neutron time-of-flight has been converted to energy is shown in

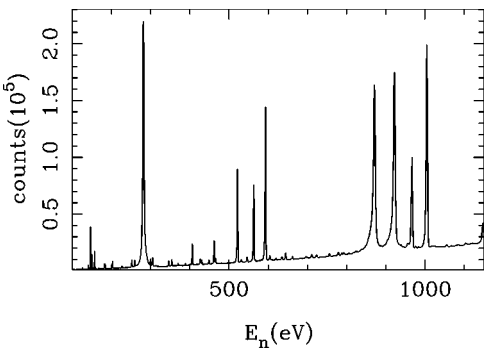

FIG. 2. A capture yield spectrum for ^{106}Pd for neutron energies from 100 to 1150 eV.

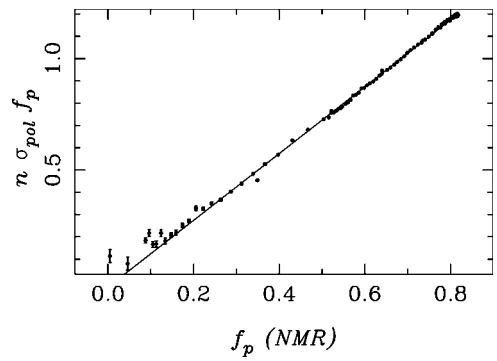

FIG. 3. Proton polarization times target thickness calibrated to the NMR measurement of proton polarization. The values along the vertical axis are determined from the ratio of transmission for polarized and unpolarized beam as discussed in the text.

Fig. 2. Detector performance is discussed in Refs. [20,21].

The metal powder target material is held in the shape of a 3.5-in diameter disk by aluminum cans with 20-mil thick front and back faces. The ^{106}Pd target has a mass of 23.328 g and is enriched to 98.51%. The ^{108}Pd target has a mass of 21.669 g and is enriched to 98.59%. Their areal densities are $n=2.11\times10^{21}$ atoms/cm^2 and $n=1.92\times10^{21}$ atoms/cm^2 for ^{106}Pd and ^{108}Pd, respectively.

The neutron spin direction is reversed every 10 s following an eight-step sequence devised to cancel effects of detector gain drifts and residual magnetic fields in the spin flipper [15]. If the beam as monitored by the ^{3}He and ^{4}He ionization chambers fluctuates by more than 8% from the average, the data for that eight-step sequence are rejected. The data from each spin state are stored in separate data areas and saved to disk every 30 min. Each 30-min run is considered as a single measurement during which time the experimental conditions should be stable. In addition to the fast spin reversal, we also change the neutron polarization by reversing the polarization direction of the proton filter.

The neutron polarization is monitored by NMR measurements of the proton target polarization. The absolute size of the neutron polarization is determined in two ways [17]. A direct calibration of the NMR measurement is performed by measuring the neutron transmission as a function of NMR signal as the proton polarization grows from zero polarization to its maximum value. The neutron transmission through the proton target is given by

$$T=T_0\cosh(n\sigma_{\rm pol}f_p), \tag{3}$$

where T and T_0 are the polarized and unpolarized transmissions, respectively, n is the proton target areal density, and f_p is the proton polarization. The polarization cross section, $\sigma_{\rm pol}$, is given by

$$\sigma_{\rm pol}=(\sigma_- - \sigma_+)/2, \tag{4}$$

where the n-p cross sections for singlet (spin $J_-=0$) and triplet (spin $J_+=1$) scattering states are given by σ_+ and σ_-, respectively. Since the neutron polarization depends on the same quantities,

$$f_n=\tanh(n\sigma_{\rm pol}f_p), \tag{5}$$

the neutron polarization f_n can be calibrated to an NMR measurement of f_p by measuring the neutron transmission for polarized and unpolarized beam. This is illustrated in Fig. 3. The expression found from the fit of the data in Fig. 3 that relates the actual $n\sigma_{\rm pol}f_p$ to the NMR measurement of the proton polarization is used to calibrate the neutron polarization to the NMR signal following Eq. (5). The neutron polarization was quite stable at about 85 and 82 % for positive and negative proton polarization, respectively. The uncertainty in the determination of the neutron polarization is 3%.

The second method for determining the neutron polarization involves a transmission measurement of the PNC effect at the 0.75-eV p-wave resonance in ^{139}La. By dividing the experimental asymmetry by the known value of the PNC asymmetry [22], one can determine the neutron polarization. This is the basis of a neutron polarimeter positioned at the end of the beam line. A 0.06534-atoms/b ^{139}La target is placed $\sim$1 m downstream from the capture detector. A 1-cm thick, 13-cm diameter, 6% by weight ^{6}Li-glass neutron detector monitors neutrons transmitted through the ^{139}La target. By counting neutrons in each helicity state in the region of the 0.75-eV p-wave resonance, a PNC asymmetry is determined from which the neutron polarization is inferred. This method provides an approximately 20% measurement of the neutron polarization per 30-min run and thus serves as a monitor of the preservation of the neutron polarization by spin transport system.

III. ANALYSIS

Discussion of the analysis is divided into three sections: fitting resonance data to determine the neutron resonance parameters, extracting the PNC asymmetries in the p-wave resonances, and determining the rms PNC matrix element and the weak spreading width Γ_w.

A. Fitting code and resonance parameters

The TRIPLE Collaboration has developed a fitting code, FITXS [23], to determine the neutron resonance parameters for neutron time-of-flight measurements carried out on flight-path 2 at MLNSC using either transmission or capture

TABLE I. PNC Asymmetries for ^{106}Pd.

E (eV) [a]	l [a]	$g\Gamma_n$ (meV) [a]	A_p (1/eV)	P (%)	$P/\Delta P$
63.43±0.04	1	0.010±0.001	1.55	0.03±0.20	0.1
146.36±0.07	1	0.53±0.04	0.406	0.035±0.045	0.8
156.88±0.07	1	0.24±0.02	0.661	0.047±0.075	0.6
300.0±0.2	1	0.18±0.02	5.80	0.19±0.24	0.8
406.7±0.3	1	0.86±0.04	0.456	−0.07±0.12	−0.6
462.3±0.3	1	1.14±0.05	0.310	−0.04±0.13	−0.3
521.9±0.4	1	6.0±0.3	0.122	−0.057±0.058	−1.0
563.4±0.5	1	5.3±0.3	0.130	−0.044±0.066	−0.7
593.4±0.5	1[b]	12.5±0.6	0.088	−0.174±0.044	−4.0
644.9±0.6	1	0.52±0.05	0.488	0.60±0.38	1.6
967.5±0.6	1	16±1	0.357	0.119±0.069	1.7
1147.9±0.9	1	4.0±0.4	0.200	0.58±0.24	2.4
1206.2±0.9	1	10.0±0.7	0.113	−0.11±0.15	−0.7
1306±1	1	3.4±0.3	0.229	0.36±0.40	0.9
1323±1	1	7.8±0.8	0.172	−0.17±0.21	−0.8
1377±1	1	2.2±0.2	1.00	−0.53±0.66	−0.8
1511±2	1	28±2	0.094	0.09±0.12	0.8
1557±2	1	1.7±0.2	0.738	−1.2±1.2	−1.0
1597±2	1	12±1	0.618	−0.17±0.22	−0.8
1624±2	1	10±1	0.229	−0.12±0.28	−0.4
1764±2	1	18±2	0.195	−0.15±0.21	0.7

[a]From Ref. [26].
[b]See text regarding the l assignment for this resonance.

detectors. The neutron cross sections are calculated using the R-matrix formalism of Reich and Moore [24]. By modeling the response of the neutron moderator at the spallation source, as well as Doppler broadening from the target material, FITXS accurately fits the observed line shape [25]. By fitting the sum of data from the two helicity states, the resonance parameters are determined for all resonances of interest. The details of the fitting procedure are discussed in Refs. [8,23,26]. The resonance parameters determined for ^{106}Pd and ^{108}Pd from transmission and capture measurements are discussed in Ref. [26], and the values for the p-wave resonances are included in Tables I and II. Figure 4 shows a sample fit of the 593.4-eV resonance in ^{106}Pd.

B. PNC asymmetries

Once the resonance parameters are determined, the data are used to obtain PNC asymmetries. After eliminating data runs with unstable run conditions, 430 30-min runs with positive proton target polarization and 354 30-min runs with negative polarization were analyzed for the ^{106}Pd target. For the ^{108}Pd target only positive polarization was used, and 350 30-min runs were analyzed.

Using the resonance parameters determined by the method described in the previous section, data from the two helicity states for each p-wave resonance are fit varying only the PNC asymmetry P. By fitting data for each resonance for every data run, a collection of P values are determined and corrected for neutron polarization. The P values then are histogramed as shown in Fig. 5. By analyzing the data in small sections (30-min runs) in this way, all nonstatistical random fluctuations in the value of the asymmetries contribute to the width of the histogram. The uncertainty in P due to random fluctuations is calculated from the standard deviation divided by the square root of the number of 30-min runs, $\sigma_{\mathrm{sdev}}/\sqrt{N}$. Calculating the uncertainty in P from the histogram in this way gives the most conservative estimate of the uncertainty in the PNC asymmetry. The size of the statistical errors for these measurements is comparable to errors in other TRIPLE measurements. The primary possible systematic error could arise from uncertainty in the neutron polarization. However, the two methods of determining the neutron polarization described above give us confidence that the neutron polarization is well known and that this systematic error is much smaller than the statistical errors. In addition, the neutron polarimeter at the end of the beam line showed stable neutron polarization throughout the run. Since the polarimeter uses the same electronics as the PNC measurements, this implies that the electronics are not producing systematic effects. The system was also frequently tested by verifying that transmission measurements of the PNC asymmetry in the 0.75-eV resonance in the ^{139}La target positioned just after the spin flipper agreed with the asymmetry measured when the target was positioned at the end of the beam line.

Finally, the PNC asymmetries are grouped by proton polarization and spin-flipper field setting so that the asymmetries can be averaged with the appropriate errors from the uncertainty in neutron polarization and corrected for spin-flipper efficiency. Tables I and II list the PNC asymmetries for the two isotopes studied. The data from the two isotopes

TABLE II. PNC Asymmetries for ^{108}Pd.

E (eV) [a]	l [a]	$g\Gamma_n$ (meV) [a]	A_p (1/eV)	P (%)	$P/\Delta P$
112.70±0.07	1	0.96±0.08	1.44	0.037±0.040	0.9
149.76±0.07	1	0.060±0.006	2.54	0.06±0.30	0.2
302.9±0.2	1	3.2±0.2	0.221	0.026±0.057	0.5
411.0±0.3	1	0.65±0.03	3.07	−0.22±0.25	−0.9
480.5±0.4	1	0.57±0.03	1.09	0.03±0.31	0.1
544.4±0.4	1	5.6±0.3	0.254	−0.036±0.090	−0.4
642.2±0.6	1	1.3±0.1	5.31	0.37±0.34	1.1
797.4±0.8	1	6.3±0.4	0.206	0.12±0.14	0.8
843.4±0.9	1	0.83±0.08	0.712	−0.45±0.65	−0.7
1082.3±0.8	1	17±1	0.151	0.09±0.12	0.7
1121±2	1	0.51±0.05	0.864	0.7±2.3	0.3
1140±2	1	0.08±0.02	2.39	−5.0±5.7	−0.9
1359±1		28±2	0.102	0.03±0.14	0.2
1456±1	1	4.5±0.5	0.543	0.45±0.54	0.8
1505±2	1	0.33±0.05	1.11	−1.2±5.2	−0.2
1523±2	1	2.8±0.3	0.393	−0.11±0.93	−0.1
1743±2	1	0.47±0.07	1.45	−8.7±4.9	−1.8
1815±2	1	2.4±0.2	0.371	1.2±1.8	0.7
2118±3	1	7.5±0.8	0.193	0.23±0.81	0.3
2165±3	1	2.6±0.3	0.243	0.4±2.5	0.2
2287±4	1	37±4	0.0418	−0.31±0.29	−1.1

[a]From Ref. [26].

show one statistically significant effect ($\Delta P/P>3$) at the 593.4-eV resonance in ^{106}Pd. The Bayesian probability for the 593.4-eV resonance to be p wave is 72%, making the orbital-angular momentum assignment inconclusive [26]. The fact that this resonance shows parity nonconservation implies that the resonance is a p wave. The subsequent analysis assumes the p-wave assignment.

C. PNC matrix elements and weak spreading width

Before determining the weak spreading width, we first determine the root-mean-squared PNC matrix element M. We use a likelihood analysis to extract the most likely value for M from the distribution of PNC effects. The likelihood function is formed from a product of Gaussian probability density functions for each p-wave resonance studied, with the width of each distribution given by a combination of M and the measurement error.

The PNC effects arise from the mixing of s- and p-wave resonances with the same spin. Since both of the targets considered here have target spin zero, only s-wave resonances with spin 1/2 are formed. However, p-wave resonances are formed with both $J=1/2$ and $J=3/2$, implying that only a fraction of the p-wave resonances can mix with the s-wave resonances to cause parity nonconservation. The spins for the Pd resonances are not known, but the resonance analysis may proceed by assigning a probability for the p-wave resonances being either $p_{1/2}$ or $p_{3/2}$ [27].

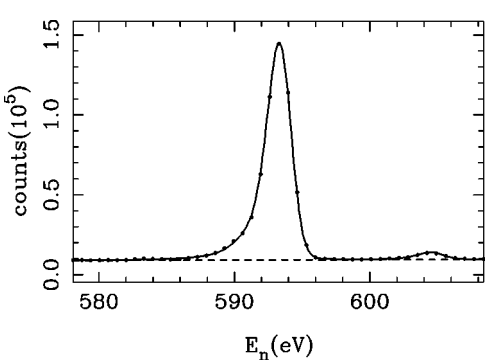

FIG. 4. Sample fit of the capture γ-ray yield versus neutron energy for the 593.4-eV resonance in ^{106}Pd. The dashed line shows a polynomial fit to the γ-ray background.

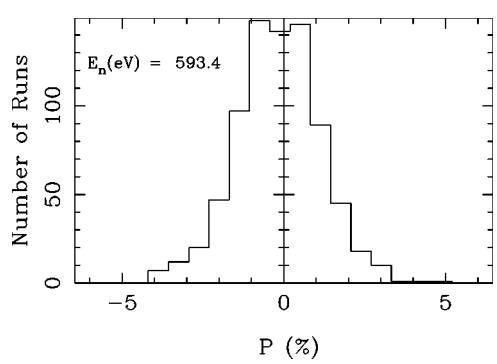

FIG. 5. Histogram of the P values for the 593.4-eV resonance in ^{106}Pd for 784 30-min runs. The mean value from the distribution is given by $P=-0.174\pm0.044$, where the uncertainty is given by $\sigma_{\rm sdev}/\sqrt{784}$.

Neglecting experimental limitations, the probability p that the p-wave resonance has spin $J=1/2$ and the probability q that the resonance has spin $J=3/2$ can be obtained from the spin distribution $F(J)$ [28]

$$F(J)\simeq\frac{2J+1}{2\sigma_c^2}\exp-\frac{(J+1/2)^2}{2\sigma_c^2}, \tag{6}$$

where the spin cutoff parameter σ_c [29] is given by

$$\sigma_c=0.98A^{0.29}, \tag{7}$$

and A is the target mass number. The probabilities p and q can be written

$$p=\frac{F(1/2)}{F(1/2)+F(3/2)} \text{ and } q=\frac{F(3/2)}{F(1/2)+F(3/2)}. \tag{8}$$

In a measurement only resonances above a certain minimum size will be observed. The fraction of the total number of p-wave resonances that are measured f can be estimated as the ratio of the number of p-wave resonances observed to the total number expected. For a spin-zero target the total number of p-wave resonances is expected to be $\sim 3\Delta E/D$, where ΔE is the range of energies analyzed and D is the s-wave level spacing. The fraction f also can be related to a minimum width parameter, $u=\gamma_{1/2}^{\min}/\langle\gamma_{1/2}\rangle$, by integrating Porter-Thomas distributions in the width parameter $y=\gamma^2/\langle\gamma^2\rangle$, for the $p_{1/2}$ and $p_{3/2}$ resonances

$$\begin{aligned} f&=p\int_{u^2}^{\infty}\frac{1}{\sqrt{2\pi y}}e^{-y/2}\,dy+q\int_{(q/p)u^2}^{\infty}\frac{1}{\sqrt{2\pi y}}e^{-y/2}dy\\ &=p\,\mathrm{erfc}(u/\sqrt{2})+q\,\mathrm{erfc}\left(\sqrt{\frac{q}{2p}}u\right). \end{aligned} \tag{9}$$

Given the experimental value for f, this equation can be solved for u. Finally, a new p' and a new $q'=1-p'$ are found from the u and f values using

$$p'=p\,\mathrm{erfc}\left(\frac{u}{\sqrt{2}}\right)\Big/ f. \tag{10}$$

Using s-wave level spacings of $D_0=217$ eV and $D_0=182$ eV for ^{106}Pd and ^{108}Pd, respectively [26], we find $p'=0.34$ and $q'=0.66$ for ^{106}Pd and $p'=0.38$ and $q'=0.62$ for ^{108}Pd.

Following Ref. [27], one can write the likelihood function for M for the case where the resonance spins are not known as

$$\begin{aligned} L(m)=P_M(m)\prod_p\Bigg[&\frac{p'}{\sqrt{2\pi(A_p^2m^2+\delta P_p^2)}}e^{-P_p^2/2(A_p^2m^2+\delta P_p^2)}\\ &+\frac{q'}{\sqrt{2\pi\delta P_p^2}}e^{-P_p^2/2\delta P_p^2}\Bigg], \end{aligned} \tag{11}$$

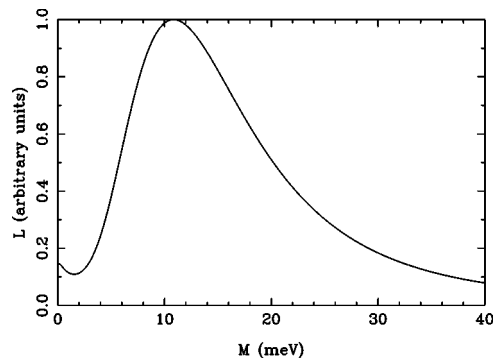

FIG. 6. Likelihood function for ^{106}Pd. The peak corresponds to $M=10.9^{+9.2}_{-5.4}$ meV. The small peak at $M=0$ is due to the influence of the large number of resonances that do not show statistically significant PNC effects.

where $P_M(m)$ is the *a priori* distribution of m. The root mean square PNC matrix element M corresponds to the value of m at which the likelihood function peaks. The likelihood function in Eq. (11) is not normalizable unless $P_M(m)$ tends to zero for large m. In practice we resolve the normalization issue by setting $P_M(m)$ equal to a constant up to some value of $m_{\max}$ and zero otherwise. For palladium, based on results in other nuclides [6–12], we used an upper limit of 40 meV. The detailed properties of the resonances are contained in the parameter A_p, defined by

$$A_p^2=\sum_s\left[\frac{2}{(E_s-E_p)}\sqrt{\frac{\Gamma_n^s}{\Gamma_n^p}}\right]^2, \tag{12}$$

where E_s, E_p, Γ_n^s, and Γ_n^p are the resonance energies and neutron widths for the s- and p-wave resonances, respectively. Note that the width of the Gaussian in the second term in Eq. (11) is due only to the uncertainty in the PNC effect. This is because the $p_{3/2}$ resonances cannot cause parity violation.

The likelihood function for ^{106}Pd is shown in Fig. 6, yielding $M=10.9^{+7.5}_{-4.5}$ meV. This implies $\Gamma_w=34^{+47}_{-28}\times10^{-7}$ eV. The uncertainties for M are obtained following Eadie [30] by solving the equation

$$\ln\left[\frac{L(m_\pm)}{L(M)}\right]=\frac{1}{2}. \tag{13}$$

One could also determine the uncertainties by numerically integrating the likelihood function and finding the most compact interval which contains 68% of the probability. With this approach we obtain $M=10.9^{+9.2}_{-5.4}$ meV, i.e., the same value of M and slightly larger errors.

The weak spreading width determined for ^{106}Pd is significantly larger than the results obtained in most other nuclides. Unusually large and small values have been observed before, as discussed by Smith *et al.* [12]. These authors find an average spreading width in the mass-100 region of $\overline{\Gamma_w}=2.56^{+0.83}_{-0.63}\times10^{-7}$ eV, where the largest value is $\Gamma_w=16.2^{+17.7}_{-08.3}\times10^{-7}$ eV (^{113}Cd) and the smallest value is $\Gamma_w=0.006^{+0.154}_{-0.003}\times10^{-7}$ eV (^{133}Cs). For ^{106}Pd the likeli-

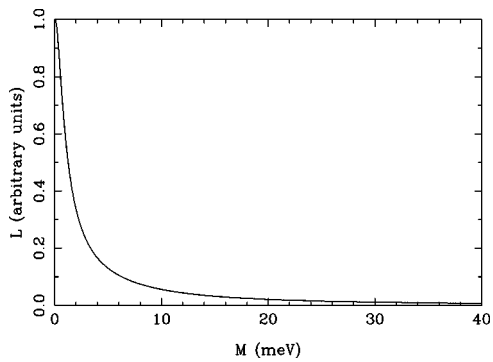

FIG. 7. Likelihood function for ^{108}Pd. The upper limit at the 68% confidence level for M is 5.8 meV. At a 95% confidence level, the upper limit on M is 26 meV.

hood function is dominated by a single effect. Figure 6 shows a small second peak near zero due to the influence of the numerous resonances that do not show parity violation. In addition, although the current analysis treats this resonance as p-wave, the l assignment for this resonance is uncertain [26]. If the 593.4-eV resonance is s wave, there must be an unresolved p-wave resonance very near in energy to the 593.4-eV resonance, with this new resonance producing the PNC asymmetry. In this case the size of the PNC matrix element is probably smaller because of the larger enhancement arising from the close proximity of the s- and p-wave resonances. However, measurements performed at the former Central Bureau for Nuclear Measurements (currently IRMM) at Geel, where the energy resolution is better than in the current measurements, did not show any additional resonances near the 593.4-eV resonance in ^{106}Pd [31].

Since we did not observe any PNC effects in the ^{108}Pd data, we expect the likelihood function to peak at zero. Using the results in Table II we find the likelihood function shown in Fig. 7. The upper limit on M of 5.8 meV is found by numerically integrating the likelihood function to 40 meV to determine the region that contain 68% probability. This corresponds to an upper limit on Γ_w of 12×10^{-7} eV. To estimate the sensitivity of the upper limit to the cutoff value $m_{\max}$ in the *a priori* distribution we performed calculations with different $m_{\max}$. For the 68% confidence intervals in M we find values of 3.2, 5.8, and 7.2 meV for $m_{\max}$ values of 10, 40, and 100 meV, respectively. We conclude that the ^{108}Pd upper limit is not very sensitive to the cutoff.

IV. SUMMARY

The capture γ-ray method has been used to measure parity nonconservation in ^{106}Pd and ^{108}Pd targets. A nearly 4π CsI detector was used to measure helicity-dependent γ yields from neutron capture of longitudinally polarized epithermal neutrons. A 10-G solenoidal field was used to preserve the neutron spins during the 50-m flight from where they are polarized to the target and detector assembly. A transmission measurement of the PNC asymmetry at 0.75-eV in ^{139}La was used as an *in situ* monitor of the neutron polarization at the target position. One statistically significant parity nonconservation effect was observed in the 593.4-eV p-wave resonance in ^{106}Pd; no effects were observed in ^{108}Pd. The ^{106}Pd result for the weak spreading width, $\Gamma_w = 34^{+47}_{-28}\times10^{-7}$ eV, suggests a local mass dependence. The ^{108}Pd results provide an upper limit on the weak spreading width, $\Gamma_w < 12\times10^{-7}$ eV, that is consistent with measurements on other targets in this mass region.

ACKNOWLEDGMENTS

This work was supported in part by the U.S. Department of Energy, Office of High Energy and Nuclear Physics, under Grant Nos. DE-FG02-97-ER41042 and DE-FG02-97-ER41033, and by the U.S. Department of Energy, Office of Research, under Contract No. W-7405-ENG-36.

[1] V. P. Alfimenkov, S. B. Borzakov, Vo Van Thuan, Yu. D. Mareev, L. B. Pikelner, A. S. Khrykin, and E. I. Sharapov, Nucl. Phys. **A398**, 93 (1983).
[2] G. E. Mitchell, J. D. Bowman, and H. A. Weidenmüller, Rev. Mod. Phys. **71**, 445 (1999).
[3] J. D. Bowman, G. T. Garvey, Mikkel B. Johnson, and G. E. Mitchell, Annu. Rev. Nucl. Part. Sci. **43**, 829 (1993).
[4] C. M. Frankle, S. J. Seestrom, N. R. Roberson, Yu. P. Popov, and E. I. Sharapov, Phys. Part. Nuclei **24**, 401 (1993).
[5] H. L. Harney, A. Richter, and H. A. Weidenmüller, Rev. Mod. Phys. **58**, 607 (1986).
[6] E. I. Sharapov *et al.*, Phys. Rev. C **59**, 1131 (1999).
[7] E. I. Sharapov *et al.*, Phys. Rev. C **59**, 1772 (1999).
[8] B. E. Crawford *et al.*, Phys. Rev. C **58**, 1225 (1998).
[9] S. L. Stephenson *et al.*, Phys. Rev. C **58**, 1236 (1998).
[10] S. J. Seestrom *et al.*, Phys. Rev. C **58**, 2977 (1998).
[11] L. Y. Lowie *et al.*, Phys. Rev. C **59**, 1119 (1999).
[12] D. A. Smith *et al.*, Phys. Rev. C **60**, 045503 (1999).
[13] Y. Masuda, T. Adachi, A. Masaike, and K. Morimoto, Nucl. Phys. **A504**, 269 (1989).
[14] E. I. Sharapov, S. A. Wender, H. Postma, S. J. Seestrom, C. R. Gould, O. A. Wasson, Yu. P. Popov, and C. D. Bowman, *Capture-Gamma Ray Spectroscopy*, edited by R. W. Hoff (AIP, New York, 1991), p. 756.
[15] N. R. Roberson *et al.*, Nucl. Instrum. Methods Phys. Res. A **326**, 549 (1993).
[16] P. W. Lisowski, C. D. Bowman, G. J. Russell, and S. A. Wender, Nucl. Sci. Eng. **106**, 208 (1990).
[17] S. I. Penttilä, J. D. Bowman, P. P. J. Delheij, C. M. Frankle, D. G. Haase, R. Mortensen, H. Postma, S. J. Seestrom, and Yi-Fen Yen, *Time Reversal Invariance and Parity Violation in Neutron Resonances*, edited by C. R. Gould, J. D. Bowman, and Yu. P. Popov (World Scientific, Singapore, 1994), p. 198.
[18] J. D. Bowman, S. I. Penttilä, and W. B. Tippens, Nucl. Instrum. Methods Phys. Res. A **369**, 195 (1996).
[19] B. E. Crawford, J. D. Bowman, and N. R. Roberson (unpublished).
[20] B. E. Crawford *et al.*, *IV International Seminar on Interactions of Neutrons with Nuclei* (JINR, Dubna, 1997), p. 268.

[21] S. J. Seestrom *et al.*, Nucl. Instrum. Methods Phys. Res. A **433**, 603 (1999).
[22] V. W. Yuan *et al.*, Phys. Rev. C **44**, 2187 (1991).
[23] Y. Matsuda, Ph.D. dissertation, Kyoto University 1997.
[24] C. W. Reich and M. S. Moore, Phys. Rev. **111**, 929 (1958).
[25] B. E. Crawford, Ph.D. dissertation, Duke University, 1997.
[26] B. E. Crawford *et al.*, Phys. Rev. C **58**, 729 (1998).
[27] J. D. Bowman, L. Y. Lowie, G. E. Mitchell, E. I. Sharapov, and Yi-Fen Yen, Phys. Rev. C **53**, 285 (1996).
[28] A. Gilbert and A. G. W. Cameron, Can. J. Phys. **43**, 1446 (1965).
[29] T. von Egidy, H. H. Schmidt, and A. N. Behkami, Nucl. Phys. **A481**, 189 (1988).
[30] W. T. Eadie, P. Drijard, F. E. James, M. Roos, and B. Sadoulet, *Statistical Methods in Experimental Physics* (North Holland, Amsterdam, 1971), p. 204.
[31] P. Staveloz, Ph.D. dissertation, Central Bureau for Nuclear Measurements, Geel, Belgium, 1981.